PHYSICAL REVIEW C **91**, 041303(R) (2015)

Magnetic response of the halo nucleus ^{19}C studied via lifetime measurement

K. Whitmore,[1,2] D. Smalley,[2] H. Iwasaki,[1,2] T. Suzuki,[3] V. M. Bader,[1,2] D. Bazin,[2] J. S. Berryman,[2] B. A. Brown,[1,2] C. M. Campbell,[4] P. Fallon,[4] A. Gade,[1,2] C. Langer,[2,5] A. Lemasson,[6] C. Loelius,[1,2] A. O. Macchiavelli,[4] C. Morse,[1,2] T. Otsuka,[2,7,8] J. Parker,[9] F. Recchia,[2,10] S. R. Stroberg,[1,2] D. Weisshaar,[2] and K. Wimmer[2,11]

[1]*Department of Physics and Astronomy, Michigan State University, East Lansing, Michigan 48824, USA*
[2]*National Superconducting Cyclotron Laboratory, Michigan State University, East Lansing, Michigan 48824, USA*
[3]*Department of Physics, Nihon University, Sakurajosui, Setagaya-ku, Tokyo 156-8550, Japan*
[4]*Nuclear Science Division, Lawrence Berkeley National Laboratory, Berkeley, California 94720, USA*
[5]*Joint Institute for Nuclear Astrophysics, Michigan State University, East Lansing, Michigan 48824, USA*
[6]*Ganil, CEA/DSM-CNRS/IN2P3, Bd Henri Becquerel, BP 55027, F-14076 Caen Cedex 5, France*
[7]*Department of Physics, University of Tokyo, Hongo, Bunkyo-ku, Tokyo 113-0033, Japan*
[8]*Center for Nuclear Study, University of Tokyo, Hongo, Bunkyo-ku, Tokyo 113-0033, Japan*
[9]*Department of Physics, Florida State University, Tallahassee, Florida 32306, USA*
[10]*Dipartimento di Fisica e Astronomia "Galileo Galilei", Universita' degli Studi di Padova, via Francesco Marzolo 8, I-35131 Padova, Italy*
[11]*Department of Physics, Central Michigan University, Mount Pleasant, Michigan 48859, USA*

(Received 27 August 2014; revised manuscript received 27 February 2015; published 20 April 2015)

The first lifetime measurement used to study the magnetic response of halo nuclei is presented. The lifetime of the first excited state of the one-neutron halo nucleus ^{19}C has been measured by two complementary Doppler-shift techniques with the Gamma-Ray Energy Tracking In-beam Nuclear Array (GRETINA). The $B(M1; 3/2^+ \rightarrow 1/2^+_{\text{g.s.}})$ strength of $3.21(25)\times10^{-3}\mu_N^2$ determined for this decay represents a strongly hindered $M1$ transition among light nuclei. Shell-model calculations predict a strong hindrance due to the near-degeneracy of the $s_{1/2}$ and $d_{5/2}$ orbitals among neutron-rich carbon isotopes, while tensor corrections and loosely bound effects are necessary to account for the remaining strength.

DOI: 10.1103/PhysRevC.91.041303 PACS number(s): 21.10.Tg, 21.60.Cs, 23.20.Lv, 27.20.+n

The electromagnetic response of atomic nuclei plays a central role in characterizing the static and dynamic nuclear properties in terms of spatial, spin, and isospin degrees of freedom. The giant resonance is one famous example, exhibiting a significant strength from coherent collective motion between protons and neutrons [1]. Depending on the excitation energy region of nuclei, the electromagnetic transition strength can provide essential information to deduce internal configurations of nuclei, quantify collectivity and deformation, and constrain the nuclear equation of state.

At the limit of nuclear stability, exotic structures can emerge due to the rearrangement of shell-model orbitals [2,3]. When the s-wave strength appears close to the threshold, quantum tunneling of valence neutrons leads to extended wave functions known as halos [4,5]. In this case, a new degree of freedom in collective modes is naïvely expected from a relative motion between the core and halo neutron, inducing so-called soft collective motions [6,7]. Nonresonant dipole excitations in light nuclei and pygmy dipole modes in medium and heavy nuclei have been extensively studied through Coulomb excitation with rare isotope beams, revealing a sizable electric dipole ($E1$) strength in the low-energy region [8]. However, the magnetic response of halo nuclei is not well understood, mainly due to difficulties in selectively inducing the magnetic excitation in intermediate-energy nuclear reactions [9]. Currently, only static magnetic properties have been studied for the one-neutron halo nucleus ^{11}Be through the β-NMR measurement of the magnetic moment [10] and hyperfine splitting measurement to deduce the magnetization radius [11]. Regarding the dynamic response, a hindered magnetic dipole ($M1$) strength has been observed for the $1/2^+ \rightarrow 3/2^+_{\text{g.s.}}$ transition in ^{17}C [12], where a possible halo structure in the excited $1/2^+$ state is discussed.

The present Rapid Communication reports the first study on the dynamic magnetic response of the neutron halo nucleus ^{19}C. In a simplistic model of the halo, an $s_{1/2}$ neutron is coupled to a 0^+ core, causing the low-energy $M1$ response to vanish due to the absence of a spin-flip partner for the $s_{1/2}$ orbital. However, the realistic picture is more complex in ^{19}C, because non-negligible core-excitation components have recently been suggested by an inclusive one-neutron removal study [13]. In this work, we quantify the magnetic transition strength in ^{19}C to identify possible hindrance, and investigate the role of shell-model configurations responsible for such a transition. The ground state has previously been studied by measurements of interaction cross sections [14], momentum distributions [15–17], Coulomb dissociation [18], and knockout reactions [13,19,20]. These results have established the one-neutron halo structure with spin and parity J^π of $1/2^+_{\text{g.s.}}$ and one-neutron separation energy S_n of 580(90) keV [21]. In addition, an excited state at ≈200 keV has been established by in-beam γ-ray studies [22,23] which propose a tentative J^π of $3/2^+$. A second possible γ-ray transition at ≈70 keV was also observed [23], suggesting a $J^\pi = 5/2^+$ state at ≈270 keV. However, this state is questioned because a $5/2^+$ state in ^{19}C was observed just above the threshold [24], and one-neutron knockout cross sections exclude a bound $5/2^+$ state [13,20]. Based on the proposed level scheme, the multipolarities of the observed transitions are expected to be $M1$, presenting an ideal case to investigate magnetic responses of halo nuclei.

In this work, the $M1$ transition strength in ^{19}C is determined through an excited-state lifetime measurement with fast rare-isotope beams using the state-of-the-art Gamma-Ray Energy Tracking In-beam Nuclear Array (GRETINA) [25]. Based on the previous γ-ray studies [23,26] and shell-model calculations [27,28], the expected lifetimes of the excited states range from the order of 10 ps to 10 ns. To cover a wide range of lifetimes, we apply two complementary Doppler-shift techniques: the line-shape and recoil-distance methods. The line-shape method [29] is based on the emission-point distribution of γ rays emitted from fast-moving reaction products and is sensitive to relatively longer lifetimes of 100 ps to 10 ns. On the other hand, the recoil distance Doppler-shift method [30] utilizes the plunger device [31], which holds the target and degrader at a precisely known distance to produce fast and slow components in the Doppler-shifted spectra. Lifetimes down to the order of 1 ps can be determined by measuring the relative γ-ray yields. The excellent energy and position resolution as well as the high detection efficiency of GRETINA allows us to make use of both methods with unprecedented sensitivity.

The experiment was performed at the Coupled Cyclotron Facility at the National Superconducting Cyclotron Laboratory (NSCL) at Michigan State University. A ^{22}Ne primary beam was accelerated to an energy of 120 MeV/nucleon and directed onto a 1081-mg/cm^2-thick ^{9}Be production target. The reaction products were collected and analyzed by the A1900 fragment separator [32] with a 2% momentum acceptance to produce a secondary beam of ^{20}N at 74 MeV/nucleon. A 750-mg/cm^2-thick Al wedge degrader was used to obtain a purity above 90%. The ^{20}N beam had a typical intensity of 1.3×10^4 pps.

The secondary beam was delivered to the experimental area, where a one-proton knockout reaction was used to populate states in ^{19}C. The plunger device [31,33] was placed at the target position of the S800 [34]. Initially, line-shape data were taken with only a 370-mg/cm^2-thick Be target. Afterward, a 1527-mg/cm^2-thick Ta foil was added 5 cm downstream of the target and used as a degrader for the recoil-distance measurement. With this degrader, the velocity of the ^{19}C beam was reduced from $v/c \approx 0.36$ to 0.32. Particle identification of reaction products was provided from energy-loss and time-of-flight measurements in the S800 [34].

De-excitation γ rays were detected with the GRETINA array [25] in coincidence with outgoing particles. GRETINA consists of seven detector modules, each containing four high-purity germanium crystals. Each crystal is divided into 36 segments, providing excellent γ-ray interaction position resolution through the signal decomposition procedure [25]. Doppler-shift corrections were made based on the γ-ray hit position in GRETINA by assuming that γ rays are emitted from the target position. The momentum-vector information of recoiling particles was obtained by the ray tracing through the S800 spectrograph and incorporated event-by-event in the Doppler-shift corrections. In order to provide a balance between the γ-ray detection efficiency and sensitivity to the varying degrees of Doppler shifts arising from different recoil velocities in the recoil-distance measurement, the target was placed about 13 cm upstream of the center of GRETINA.

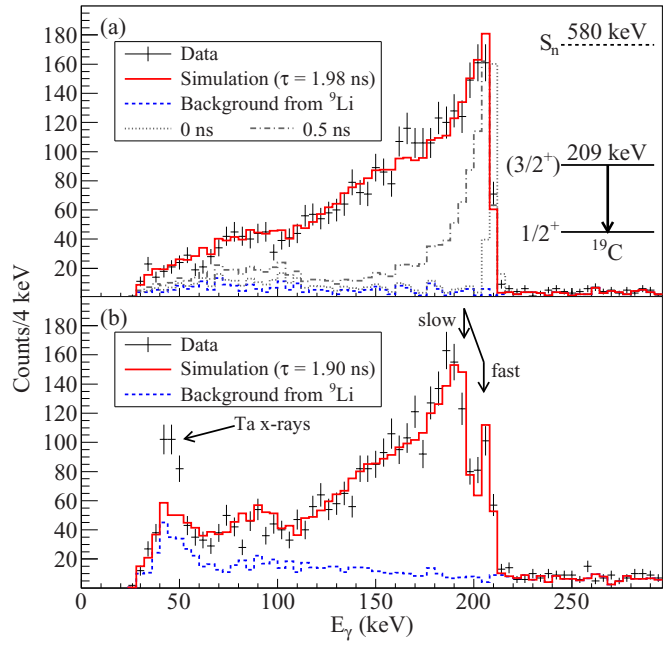

FIG. 1. (Color online) Data from (a) line-shape and (b) recoil-distance measurements are compared to simulated spectra (solid red histograms) which include scaled ^{9}Li spectra as background contributions (dashed blue histograms). In (a), the dotted (dot-dashed) gray histogram shows a reference spectrum simulated with a mean lifetime of 0 ns (0.5 ns).

This resulted in four detectors being located around 40° and three detectors around 65° .

The Doppler-shift corrected γ-ray spectra from the line-shape and recoil-distance measurements are shown in Figs. 1(a) and 1(b), respectively. The multiplicity M=1 is chosen to improve the signal-to-noise ratio. The γ-ray peaks associated with the decay from the first excited state at 209(2) keV are clearly visible in both spectra with characteristic spectral shapes which provide a means to constrain the decay lifetime. In both Figs. 1(a) and 1(b), the peaks show a broad low-energy tail extending down to about 100 keV. The moderate slope in the spectra indicates the γ decays occur while ^{19}C recoils are moving along the beam path surrounded by GRETINA. This means the decay lifetime is on the order of nanoseconds, because the detector coverage extends about 30 cm downstream of the target, corresponding to a flight time of 3 ns at the ^{19}C recoil velocity. Concerning the recoil-distance spectrum shown in Fig. 1(b), the two-peak structure is evident at around 200 keV with the fast and slow components arising from the different recoil velocities. Since the γ-ray yield is much larger for the slow component, the lifetime is likely longer than the flight time (0.5 ns) of recoils passing through the target-degrader separation of 5 cm. A transition from a possible state near 270 keV is not significantly observed in the present work. A γ-γ analysis gated on the 209-keV transition places an upper limit of 10% on the possible feeding.

The lifetime was determined through χ^2 minimization by comparing data to simulated spectra [29,35]. The simulation utilizes the GEANT4 package and incorporates the geometry

of GRETINA [33]. The variable parameters used in the fits are the lifetime of the state and the amplitudes of both the spectrum and the background contribution. In this study, the spectrum in coincidence with ^{9}Li recoils was used as the background, instead of the exponential background typically assumed, in order to separate the summed contributions from the background and lifetime effects and properly incorporate the detector response close to the threshold. In ^{9}Li, the only γ transition is from the state at 2.7 MeV, and the low-energy region of the spectrum should be dominated by background.

The best-fit results are shown in Fig. 1. The fit was made using the energy region above 100 keV. This corresponds to roughly 130 keV in the laboratory frame, where the consistency with simulation was verified with standard sources. The mean lifetime (τ) of the first excited state was determined to be 1.98(10) ns and 1.90(10) ns from the line-shape and recoil-distance data, respectively, where the errors are statistical only. Systematic errors stemming from uncertainties in geometry and beam properties are at most 3% for either measurement. For the recoil-distance data, additional ambiguities arise from reactions producing ^{19}C in the degrader, which introduce background contributions in the lifetime measurement. The target/degrader reaction yield ratio R assumed in the present simulation is 4.6(14), which is estimated from the ratios deduced in previous experiments which utilized analogous one-proton knockout reactions from nitrogen projectiles [36,37]. The large R in this measurement results in a small additional error of 2%. By adding the statistical and systematic errors in quadrature, the results are deduced to be 1.98(12) and 1.90(13) ns for the two measurements. Because the two results are consistent, the adopted value is determined to be 1.94(15) ns by taking the average, where the error also includes the difference (4%) between the two results.

Assuming a pure $M1$ transition, the $B(M1)$ strength for the 209-keV transition can be determined to be $3.21(25)\times10^{-3}\mu_N^2$ or $1.79(14)\times10^{-3}$ Weisskopf units (W.u.). If there is an admixture from the $E2$ multipolarity in this decay, the $B(M1)$ strength is reduced accordingly. However, the effect is expected to be negligible in this case due to the $1/E^{2L+1}$ dependence of the partial lifetimes. In this mass region, the largest $E2$ transition strengths connecting to ground states are about 20 W.u. [39]. With this strength assumed, the $B(M1)$ is reduced by only 6%. In fact, the $E2$ strengths for the $2^+ \rightarrow 0^+$ transitions in neighboring even carbon isotopes are only 1–3 W.u. [36,37,40], so the $E2$ contribution in ^{19}C may be safely ignored. A possible spin and parity assignment of $5/2^+$ for the 209-keV state would require a pure $E2$ transition for the decay to the $1/2^+$ ground state, which would result in a $B(E2)$ of 350 W.u., far beyond the recommended upper limit [39]. Thus the present measurement supports the $3/2^+$ assignment previously proposed for the first excited state in ^{19}C.

To investigate the degree of the $M1$ hindrance in ^{19}C, the present result is compared to existing data for $M1$ decay strengths in the mass region $A < 40$ in Fig. 2 [38]. For reference, the analogous decay strength measured in the $1/2^+ \rightarrow 3/2^+_{\text{g.s.}}$ transition in ^{17}C is also plotted [12]. As is clear in Fig. 2(a), the $M1$ transition in ^{19}C is among the smallest

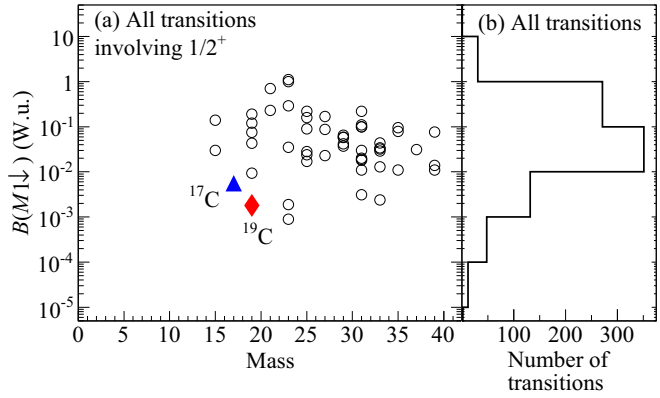

FIG. 2. (Color online) Experimental decay strengths in the mass region $A < 40$ are plotted in W.u. for (a) the $M1$ transitions involving the $1/2^+$ state(s) and (b) all $M1$ transitions [38]. The red diamond highlights the present value for the $3/2^+ \rightarrow 1/2^+$ transition in ^{19}C, while the $1/2^+ \rightarrow 3/2^+_{\text{g.s.}}$ decay strength in ^{17}C [12] is shown by the blue triangle.

strengths observed for those $M1$ transitions that involve $1/2^+$ states, even below that of ^{17}C (5.7×10^{-3} W.u.) [12]. Even when compared to all transitions in this mass region as shown in Fig. 2(b), the $M1$ hindrance in ^{19}C still remains evident, indicative of the unusual structure of ^{19}C. In Fig. 2(a), two points at $A = 23$ are also visible, denoting the $1/2^+ \rightarrow 3/2^+_{\text{g.s.}}$ transitions in the mirror nuclei ^{23}Na and ^{23}Mg. These are considered to be interband transitions between Nilsson orbits [2 1 1 1/2] and [2 1 1 3/2] of well-deformed nuclei [41]. In a shell-model picture, the hindrance is due to a large cancellation between the orbital and spin contributions to the $M1$ strength [42].

Shell-model calculations were performed and compared to the data as a way to understand the origin of the hindrance as well as the remaining strength. Two effective interactions, SFO-tls [27] and Yuan [43], are used in the psd model space [27]. Calculations with the WBP interaction [28] were also performed. The SFO-tls interaction is developed based on the PSDMK2 interaction [27] with improvements to the tensor component, which affects magnetic properties directly [27]. The Yuan interaction [43] incorporates a monopole-based universal interaction including the bare $\pi+\rho$ tensor force for the $\langle psd|V|psd\rangle$ and $\langle pp|V|sdsd\rangle$ matrix elements which have not been well studied in phenomenological effective interactions.

The calculated results for the $B(M1)$ strength and the ^{19}C level scheme are shown in Figs. 3(a) and 3(b) respectively. The $B(M1)$ values are first obtained with the effective g factors $\delta g_\ell^{\text{IV}} = 0.15$ and $g_s^{\text{IV,eff}}/g_s^{\text{IV}} = 0.95$ as shown by the solid bars in Fig. 3(a). All three calculations (WBP, SFO-tls, Yuan) consistently show strongly hindered strengths for the $3/2^+ \rightarrow 1/2^+$ transition, even below the measured value. However, the level of agreement is improved if one employs the modified $M1$ operator (striped bars) with the effective g factors $g_{\ell p} = 1.175$, $g_{\ell n} = -0.106$, $g_{sp} = 5$, $g_{sn} = -3.5$, $g_{tp} = 0.26$, and $g_{tn} = -0.17$ [42]. Within this modified operator, the tensor effective g factors allow

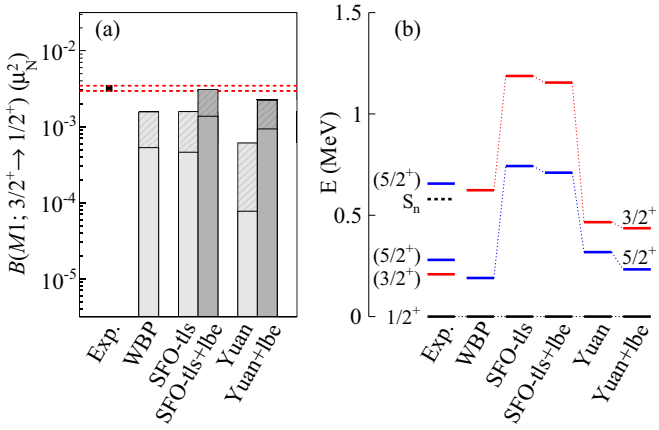

FIG. 3. (Color online) Comparison of the data with shell-model predictions (see text) for (a) the $B(M1)$ strength for the $3/2^+ \rightarrow 1/2^+$ transition and (b) the level scheme of ^{19}C. In (a), the solid bars are the results obtained with $g_s^{\mathrm{IV,eff}}/g_s^{\mathrm{IV}} = 0.95$ and $\delta g_\ell^{\mathrm{IV}} = 0.15$ [27], while the striped bars are obtained with the modified $M1$ operator as described in the text [42]. The level scheme in (b) shows the $5/2^+$ states (blue) suggested by previous experiments [23,24] in addition to the presently studied $3/2^+$ state (red).

the ℓ-forbidden transitions. Concerning the level scheme, all three interactions reproduce the ground-state spin and parity of $1/2^+$. The order of the excited levels is inverted in all calculations, while the degeneracy among all three states is well reproduced, particularly by the Yuan calculation. Since it has been found that the $B(M1)$ strength is especially sensitive to a few matrix elements, such as $\langle s_{1/2}d_{5/2}|V|d_{5/2}d_{3/2}\rangle$ and $\langle s_{1/2}d_{5/2}|V|s_{1/2}d_{3/2}\rangle$, possible additional improvements are considered by adjusting those matrix elements. As discussed in Ref. [27], the above two matrix elements in the $J = 2$ and $T = 1$ channel are reduced by 20% to simulate loosely bound effects (denoted +lbe in Fig. 3 and hereafter). As shown in Fig. 3, this modification further improves predictions of the $B(M1)$ strength for the SFO-tls and Yuan interactions, without causing significant impacts on the energy levels.

The observed $M1$ hindrance can be ascribed to the lowering of the $s_{1/2}$ orbital and resultant proximity to the $d_{5/2}$ orbital characteristic of weakly bound nuclei. The degeneracy of these orbitals is supported by all the calculations, as demonstrated by the compressed level schemes shown in Fig. 3(b). Among all calculations, the primary configurations of the valence neutrons in the ground and first excited states in ^{19}C are given as follows:

$$
\begin{aligned}
|^{19}\mathrm{C}(1/2^+)\rangle &= \alpha\left|(d_{5/2})^4_{J=0^+}\otimes(s_{1/2})\right\rangle + \cdots, \\
|^{19}\mathrm{C}(3/2^+)\rangle &= \beta\left|(d_{5/2})^4_{J=2^+}\otimes(s_{1/2})\right\rangle \\
&\quad + \gamma\left|(d_{5/2})^3_{J=3/2^+}\otimes(s_{1/2})^2\right\rangle + \cdots, \qquad (1)
\end{aligned}
$$

where the internal configuration of ^{14}C(0^+) is $|(p_{3/2})^8\otimes(p_{1/2})^2\rangle$. For the WBP and Yuan(+lbe) interactions, the amplitudes are about $\alpha^2 \approx 0.48$, $\beta^2 \approx 0.29$, and $\gamma^2 \approx 0.26$, while the SFO-tls(+lbe) gives about $\alpha^2 \approx 0.40$, $\beta^2 \approx 0.26$, and $\gamma^2 \approx 0.23$. The agreement between these calculations clearly shows the prevalence of the $s_{1/2}$ and $d_{5/2}$ components in both the ground and excited states. If the neutron configurations are restricted to the $(s_{1/2}d_{5/2})^n$ space above the 0^+ core, the only possible configurations for the $1/2^+$ and $3/2^+$ states in ^{19}C are those listed in Eq. (1), which lead to zero $M1$ strength. More generally, all possible configurations for the $(s_{1/2}d_{5/2})^5$ space are (a) $(d_{5/2})^5$ $J{=}5/2^+$; (b) $(d_{5/2})^4_{J=0^+}\otimes(s_{1/2})$ $J = 1/2^+$; (c) $(d_{5/2})^4_{J=2^+}\otimes(s_{1/2})$ $J = 3/2^+$, $5/2^+$; (d) $(d_{5/2})^4_{J=4^+}\otimes(s_{1/2})$ $J = 7/2^+$, $9/2^+$; and (e) $(d_{5/2})^3\otimes(s_{1/2})^2$ $J = 3/2^+, 5/2^+, 9/2^+$. The $B(M1)$ strength is zero between all pairs of these configurations except for the spin-flip transitions between the $3/2^+$ and $5/2^+$ states in (c), and the $7/2^+$ and $9/2^+$ states in (d). For other transitions, the $\Delta\ell = 2$ s-d transition is involved [note that the $M1$ strength between the $3/2^+$ and $5/2^+$ states in (e) is also zero because they are within the identical $(d_{5/2})^3$ space]. This is the primary mechanism responsible for the suppressed $B(M1)$ values in ^{19}C. Other components to the wave functions could allow finite strengths, but the total $B(M1)$ remains diminished due to their smaller amplitudes in addition to cancellation among the different $M1$ components. A decomposition of the $M1$ strength into the individual matrix elements for the proton and neutron orbital, spin, and tensor components using the SFO-tls+lbe interaction is shown in Fig. 4. Thus the prominence of the $s_{1/2}$ and $d_{5/2}$ orbitals reduces the $M1$ strength down to the level of 10^{-3} μ_N^2, where the contributions from the ℓ-forbidden transition between the $s_{1/2}$ and $d_{3/2}$ orbitals become noticeable.

In summary, we have measured the lifetime of the first excited $3/2^+$ state in the one-neutron halo nucleus ^{19}C. The resultant $B(M1)$ strength amounts to $3.21(25)\times10^{-3}$ μ_N^2, which represents one of the weakest $M1$ transitions among light nuclei. In this nucleus, the lowering of the neutron $s_{1/2}$ orbital is responsible for the halo formation, and considerations based on the shell model suggest that the resultant $s_{1/2}$-$d_{5/2}$ degeneracy suppresses the $M1$ transition. In the limit that only $s_{1/2}$ and $d_{5/2}$ orbitals contribute, the neutron configurations

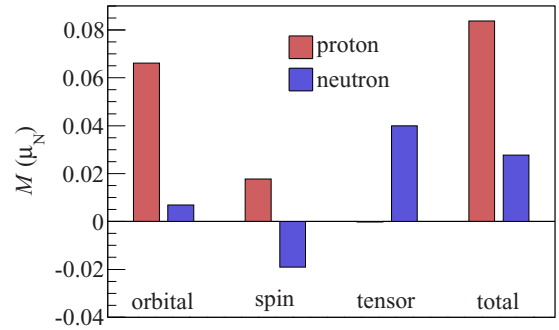

FIG. 4. (Color online) Results of the SFO-tls+lbe interaction [27] for the $M1$ strength between the $3/2^+$ and $1/2^+$ states in ^{19}C, calculated with the effective g factors as described in the text [42]. The plot shows, from left to right, the values of the individual matrix elements (M) for the orbital, spin, tensor, and total components of the $M1$ operator for both the protons (red) and neutrons (blue). The proton tensor component has a negligible value compared to the other components.

are restricted to those components shown explicitly in Eq. (1), leading to a vanished $M1$ transition. Calculations based on *ab initio* approaches are now becoming possible in this mass region [44,45], and it will be interesting to compare those calculations to the present data. This work presents a novel approach to study magnetic responses of halo nuclei through lifetime measurements with fast rare-isotope beams. It also establishes criteria for hindered magnetic dipole responses of s-wave halo nuclei, motivating future measurements in heavier systems. Very recently, the occurrence of deformed p-wave halos has been proposed for neon and magnesium isotopes [46,47], presenting intriguing cases for such studies.

The authors thank the beam line operators at the Coupled Cyclotron Facility for the delivery of the radioactive beam. We also thank D. Suzuki for fruitful discussions. This work is supported by the National Science Foundation (NSF) under PHY-1102511, by the Department of Energy (DOE) National Nuclear Security Administration under award number DE-NA0000979, and by Grants-in-Aid for Scientific Research (C) 22540290 of the Ministry of Education, Culture, Sports, Science and Technology of Japan. GRETINA was funded by the U.S. DOE Office of Science. Operation of the array at NSCL is supported by NSF under Cooperative Agreement PHY-1102511 (NSCL) and DOE under Grant No. DE-AC02-05CH11231 (LBNL).

[1] J. Speth and A. van der Woude, Rep. Prog. Phys. **44**, 719 (1981).
[2] T. Otsuka, T. Suzuki, R. Fujimoto, H. Grawe, and Y. Akaishi, Phys. Rev. Lett. **95**, 232502 (2005). T. Otsuka, Phys. Scr., T **152**, 014007 (2013).
[3] O. Sorlin and M.-G. Porquet, Prog. Part. Nucl. Phys. **61**, 602 (2008).
[4] I. Tanihata *et al.*, Phys. Rev. Lett. **55**, 2676 (1985).
[5] P. G. Hansen and B. Jonson, Europhys. Lett. **4**, 409 (1987).
[6] K. Ikeda, Nucl. Phys. A **538**, 355c (1992).
[7] H. Esbensen and G. F. Bertsch, Nucl. Phys. A **542**, 310 (1992).
[8] T. Aumann and T. Nakamura, Phys. Scr., T **152**, 014012 (2013).
[9] C. A. Bertulani and G. Baur, Phys. Rep. **163**, 299 (1988).
[10] W. Geithner *et al.*, Phys. Rev. Lett. **83**, 3792 (1999).
[11] A. Takamine *et al.*, Phys. Rev. Lett. **112**, 162502 (2014).
[12] D. Suzuki *et al.*, Phys. Lett. B **666**, 222 (2008).
[13] N. Kobayashi *et al.*, Phys. Rev. C **86**, 054604 (2012).
[14] R. Kanungo *et al.*, Nucl. Phys. A **677**, 171 (2000).
[15] D. Bazin *et al.*, Phys. Rev. Lett. **74**, 3569 (1995).
[16] F. M. Marqués *et al.*, Phys. Lett. B **381**, 407 (1996).
[17] T. Baumann *et al.*, Phys. Lett. B **439**, 256 (1998).
[18] T. Nakamura *et al.*, Phys. Rev. Lett. **83**, 1112 (1999).
[19] V. Maddalena *et al.*, Phys. Rev. C **63**, 024613 (2001).
[20] A. Ozawa *et al.*, Phys. Rev. C **84**, 064315 (2011).
[21] M. Wang *et al.*, Chin. Phys. C **36**, 1603 (2012).
[22] M. Stanoiu *et al.*, Eur. Phys. J. A **20**, 95 (2004).
[23] Z. Elekes *et al.*, Phys. Lett. B **614**, 174 (2005).
[24] M. Thoennessen *et al.*, Nucl. Phys. A **912**, 1 (2013).
[25] S. Paschalis *et al.*, Nucl. Instrum. Methods Phys. Res., Sect. A **709**, 44 (2013).
[26] R. Kanungo *et al.*, Nucl. Phys. A **757**, 315 (2005).
[27] T. Suzuki and T. Otsuka, Phys. Rev. C **78**, 061301(R) (2008).
[28] E. K. Warburton and B. A. Brown, Phys. Rev. C **46**, 923 (1992).
[29] A. Lemasson *et al.*, Phys. Rev. C **85**, 041303(R) (2012).
[30] A. Dewald *et al.*, Prog. Part. Nucl. Phys. **67**, 786 (2012).
[31] A. Dewald *et al.* (unpublished).
[32] D. J. Morrissey *et al.*, Nucl. Instrum. Methods Phys. Res., Sect. B **204**, 90 (2003).
[33] H. Iwasaki *et al.*, Phys. Rev. Lett. **112**, 142502 (2014).
[34] D. Bazin *et al.*, Nucl. Instrum. Methods Phys. Res., Sect. B **204**, 629 (2003).
[35] P. Adrich *et al.*, Nucl. Instrum. Methods Phys. Res., Sect. A **598**, 454 (2009).
[36] P. Voss *et al.*, Phys. Rev. C **86**, 011303(R) (2012).
[37] M. Petri *et al.*, Phys. Rev. C **86**, 044329 (2012).
[38] Evaluated Nuclear Structure Data File (ENSDF), http://www.nndc.bnl.gov/ensdf.
[39] P. M. Endt, At. Data Nucl. Data Tables **55**, 171 (1993).
[40] M. Petri *et al.*, Phys. Rev. Lett. **107**, 102501 (2011).
[41] Y. Fujita *et al.*, Phys. Rev. C **66**, 044313 (2002).
[42] W. A. Richter, S. Mkhize, and B. A. Brown, Phys. Rev. C **78**, 064302 (2008).
[43] C. Yuan, T. Suzuki, T. Otsuka, F. Xu, and N. Tsunoda, Phys. Rev. C **85**, 064324 (2012).
[44] G. R. Jansen, J. Engel, G. Hagen, P. Navratil, and A. Signoracci, Phys. Rev. Lett. **113**, 142502 (2014).
[45] S. Pastore, S. C. Pieper, R. Schiavilla, and R. B. Wiringa, Phys. Rev. C **87**, 035503 (2013).
[46] T. Nakamura *et al.*, Phys. Rev. Lett. **112**, 142501 (2014).
[47] N. Kobayashi *et al.*, Phys. Rev. Lett. **112**, 242501 (2014).